AIAA JOURNAL
Vol. 40, No. 6, June 2002

Damping Analysis of Composite Plates with Zig-Zag Triangular Element

D. G. Lee* and J. B. Kosmatka†
University of California, San Diego, La Jolla, California 92093-0085

A three-node flat triangular element incorporating layerwise zig-zag theory is developed that is suitable for analyzing damped laminated composite structures. By the use of an interdependent kinematic relation, the higher-order shear rotations are replaced by in-plane displacements, a transverse displacement, and section rotations, which result in three translations and two rotations. Natural frequencies and modal loss factors of cantilevered laminated plates with embedded damping layers are calculated with the zig-zag triangular element and compared to the experimental results and MSC/NASTRAN results using a layered combination of plate and solid elements. Frequencies and corresponding loss factors of symmetric and antisymmetric damped laminated cantilever plates as a function of fiber angle are also calculated.

I. Introduction

INTEGRALLY embedding a viscoelastic damping layer within a laminated composite structure is a very effective way of suppressing fatigue-sensitive flexural vibrations. Embedded damping layers dissipate vibratory energy, predominantly through shear during flexural motion. There is a need to develop an accurate laminated theory that accounts for arbitrary ply thickness variations, extreme rigidity differences, and ply loss factor variations in laminated structures with embedded viscoelastic layers.

Yan and Dowell,[1] Rao and Nakra,[2] Douglas and Yang,[3] Miles and Reinhall,[4] and Barrett[5] developed simple differential equations for sandwich plates for a constraining layer damping model. Alam and Asnani[6,7] developed a general multilayered plate model consisting of an arbitrary number of alternating stiff and soft layers of orthotropic materials. Johnson and Kienholz[8] analyzed a sandwich plate with a damping core by a modal strain energy method implemented in NASTRAN. Malhotra et al.[9] studied the effect of fiber orientation on the vibration and damping behavior of thin orthotropic triangular plates. Saravanos and Pereira[10] and Saravanos[11] incorporated discrete-layer laminate theory (DLLT) into the modeling of composite structures with interlaminar damping layers. DLLT assumes a discrete yet piecewise continuous displacement field through the thickness. The number of unknowns of DLLT depends on the number of subdivision through the thickness. Hence, DLLT requires enormous computing costs to predict accurately three-dimensional stress distribution, which is vitally important for the damping analysis of laminated composite structures with embedded viscoelastic layers.

Di Sciuva[12–14] developed the higher-order zig-zag displacement theory based on the refined higher-order displacement field that satisfies a priori traction-free boundary conditions superimposed by the zig-zag displacement field. Di Sciuva[15] derived a higher-order zig-zag displacement theory and developed a three-node, conforming, triangular element that has 10 nodal degrees of freedom (DOF): two in-plane displacements, two shear rotations, and a transverse displacement with its first and second derivatives (section rotations and curvatures). This element has been successfully applied to the static bending and free vibration behavior of composite plates. Cho and Parmerter[16] derived an efficient higher-order zig-zag displacement field and developed a triangular bending element based on the shape functions suggested by Specht.[17] This resulted in a nonconforming element having five nodal DOF: two shear rotations, a transverse displacement, and the two section rotations. Lee,[18] Lee and Waas,[19,20] and Lee et al.[21] developed sector zig-zag element and studied the effect of fiber orientation on the stability and transient response of spinning composite disks under frictional load. Averill[22] and Averill and Yip[23] have developed the higher-order zig-zag displacement field and corresponding beam elements and accurately predicted the stress distribution through the thickness of laminated structures.

In the present work, a three-node flat triangular element using the zig-zag theory and interdependent kinamatic relations is developed. With interdependent kinematic relations, the higher-order shear rotation DOF are replaced by the in-plane displacements, a transverse displacement, and the section rotations. The remaining transverse displacement and section rotations are interpolated based on shape functions suggested by Specht[17] that result in three translations and two rotations at each vertex of the triangular element. Natural frequencies and modal loss factors of a cantilevered rectangular laminated plate with an embedded damping layer are calculated with the present three-node zig-zag triangular element. Various fiber orientations, border materials, and damping patch sizes are investigated. Current results are compared to experimental results and analytical (MSC/NASTRAN) results using a layered combination of plate and solid elements. Frequencies and corresponding loss factors of symmetric and antisymmetric damped laminated cantilever plates as a function of fiber angle are also calculated with the zig-zag triangular element.

II. Theoretical Development

Consider a plate composed of multiple layers. The improved layerwise zig-zag displacement fields for the kth layer are defined as in Ref. 24:

$$u^{(k)} = u_0 - z\frac{\partial w_0}{\partial x} + h_{11}^{(k)}\phi_x + h_{12}^{(k)}\phi_y$$

$$v^{(k)} = v_0 - z\frac{\partial w_0}{\partial y} + h_{21}^{(k)}\phi_x + h_{22}^{(k)}\phi_y$$

$$w^{(k)} = w_0 \tag{1}$$

where u_0 and v_0 are the in-plane displacements, w_0 is a transverse displacement, ϕ_x and ϕ_y are the higher-order shear rotations, and $h_{11}^{(k)}$, $h_{12}^{(k)}$, $h_{21}^{(k)}$, $h_{22}^{(k)}$ are defined as follows:

Received 21 May 2001; revision received 20 November 2001; accepted for publication 24 December 2001.

*Postdoctoral Researcher, Department of Structural Engineering; currently BK21 Postdoctoral Research Associate, School of Mechanical and Aerospace Engineering, Seoul National University, Institute of Advanced Machinery and Design, Building 136-1, Room 2201, San 56-1 Shinlim-dong, Kwanak-gu, Seoul 151-742, Republic of Korea; dglee@snu.ac.kr.

†Professor, Department of Structural Engineering. Associate Fellow AIAA.

$$h_{11}^{(k)} = z^2 + z^3 f_1 + \sum_{i=1}^{k-1}(z - z_i)(a_{2i} + a_{3i} f_1 + b_{3i} f_3)$$

$$h_{12}^{(k)} = z^3 f_2 + \sum_{i=1}^{k-1}(z - z_i)(a_{3i} f_2 + b_{2i} + b_{3i} f_4)$$

$$h_{21}^{(k)} = z^3 f_3 + \sum_{i=1}^{k-1}(z - z_i)(c_{2i} + c_{3i} f_1 + d_{3i} f_3)$$

$$h_{22}^{(k)} = z^2 + z^3 f_4 + \sum_{i=1}^{k-1}(z - z_i)(c_{3i} f_2 + d_{2i} + d_{3i} f_4) \qquad (2)$$

where $f_1, f_2, f_3, f_4, a_{2i}, a_{3i}, b_{2i}, b_{3i}, c_{2i}, c_{3i}, d_{2i}, d_{3i}$ are evaluated as shown in Appendix A.

A. Interdependent Kinematic Relations

In the case of symmetric layups, the in-plane displacement distribution through the thickness should be symmetric about the midplane, which suggests that integration through the thickness of in-plane displacements ($u^{(k)}$, $v^{(k)}$), multiplied by normal material constants in each direction set to zero, gives the interdependent kinematic relation between the higher-order shear rotations (ϕ_x, ϕ_y), in-plane displacements (u_0, v_0), the transverse displacement w_0, and the section rotations ($\partial w_0/\partial x$, $\partial w_0/\partial y$) as follows:

$$\sum_{k=1}^{N} \int_{z_{k-1}}^{z_k} C_{11}^{(k)} \left(u - z\frac{\partial w}{\partial x} + h_{11}^{(k)}\phi_x + h_{12}^{(k)}\phi_y \right) \mathrm{d}z = 0$$

$$\sum_{k=1}^{N} \int_{z_{k-1}}^{z_k} C_{22}^{(k)} \left(v - z\frac{\partial w}{\partial y} + h_{21}^{(k)}\phi_x + h_{22}^{(k)}\phi_y \right) \mathrm{d}z = 0 \qquad (3)$$

after the integration through thickness is performed, Eq. (3) is read as

$$A_{11}u - B_{11}\frac{\partial w}{\partial x} + Q_{11}\phi_x + Q_{12}\phi_y = 0$$

$$A_{22}v - B_{22}\frac{\partial w}{\partial y} + Q_{23}\phi_x + Q_{24}\phi_y = 0 \qquad (4)$$

where (A, B, Q) are defined in Appendix B. Equation (4) is rearranged for ϕ_x and ϕ_y in terms of u_0, v_0, $\partial w_0/\partial x$, and $\partial w_0/\partial y$ as

$$\begin{Bmatrix} \phi_x \\ \phi_y \end{Bmatrix} = \begin{bmatrix} -c_x^1 & c_x^3 & c_x^2 & -c_x^4 \\ c_y^1 & -c_y^3 & -c_y^2 & c_y^4 \end{bmatrix} \begin{Bmatrix} u_0 \\ v_0 \\ \dfrac{\partial w_0}{\partial x} \\ \dfrac{\partial w_0}{\partial y} \end{Bmatrix} \qquad (5)$$

where the constants in Eq. (5) are defined as

$$c_x^1 = \frac{A_{11}Q_{24}}{D_e}, \qquad c_x^2 = \frac{B_{11}Q_{24}}{D_e}, \qquad c_x^3 = \frac{A_{22}Q_{12}}{D_e}$$

$$c_x^4 = \frac{B_{22}Q_{12}}{D_e}, \qquad c_y^1 = \frac{A_{11}Q_{23}}{D_e}, \qquad c_y^2 = \frac{B_{11}Q_{23}}{D_e}$$

$$c_y^3 = \frac{A_{22}Q_{11}}{D_e}, \qquad c_y^4 = \frac{B_{22}Q_{11}}{D_e}$$

$$D_e = Q_{11}Q_{24} - Q_{12}Q_{23} \qquad (6)$$

B. Strain–Displacement Relations

The linear strain–displacement relations for the kth layer in a Cartesian coordinate system are defined as follows:

$$\begin{Bmatrix} e_x \\ e_y \\ \gamma_{xy} \end{Bmatrix}^{(k)} = \begin{bmatrix} 1 & 0 & 0 & -z & 0 & 0 & h_{11}^{(k)} & h_{12}^{(k)} & 0 & 0 \\ 0 & 1 & 0 & 0 & -z & 0 & 0 & 0 & h_{21}^{(k)} & h_{22}^{(k)} \\ 0 & 0 & 1 & 0 & 0 & -z & h_{21}^{(k)} & h_{22}^{(k)} & h_{11}^{(k)} & h_{12}^{(k)} \end{bmatrix} \{\varepsilon\} \qquad (7)$$

$$\begin{Bmatrix} \gamma_{yz} \\ \gamma_{xz} \end{Bmatrix}^{(k)} = \begin{bmatrix} h_{21,z}^{(k)} & h_{22,z}^{(k)} \\ h_{11,z}^{(k)} & h_{12,z}^{(k)} \end{bmatrix} \{\gamma\} \qquad (8)$$

and the general membrane-bending strain vector $\{\varepsilon\}$ using the interdependent kinematic relation (5) is defined as

$$\{\varepsilon\} = [T_B]\{\bar{\varepsilon}\} \qquad (9)$$

where $[T_B]$ is defined in Appendix C and $\{\bar{\varepsilon}\}$ is

$$\{\bar{\varepsilon}\} = \left\{ \frac{\partial u_0}{\partial x}, \frac{\partial v_0}{\partial x}, \frac{\partial u_0}{\partial y}, \frac{\partial v_0}{\partial y}, \frac{\partial^2 w_0}{\partial x^2}, \frac{\partial^2 w_0}{\partial y^2}, \frac{\partial^2 w_0}{\partial x \partial y} \right\}^T \qquad (10)$$

The general higher-order shear rotation vector $\{\gamma\}$ using the interdependent kinematic relation (5) is defined as

$$\{\gamma\} = [T_S]\{\bar{\gamma}\} \qquad (11)$$

where $[T_S]$ is defined in Appendix C and $\{\bar{\gamma}\}$ is

$$\{\bar{\gamma}\} = \left\{ u_0, v_0, \frac{\partial w_0}{\partial x}, \frac{\partial w_0}{\partial y} \right\}^T \qquad (12)$$

C. Complex Constitutive Relations

The reduced-transformed complex orthotropic stress–strain relation under the plane stress assumption ($\sigma_z = 0$) for any individual layer (kth layer) is defined as

$$\{\sigma\}^{(k)} = \left([\bar{C}]^{(k)} + i[\bar{C}]^{(k)}[\bar{\eta}]^{(k)} \right)\{e\}^{(k)} \qquad (13)$$

where the stress and the linear elastic strain are read as

$$\{\sigma\}^{(k)} = \{\sigma_x, \sigma_y, \tau_{yz}, \tau_{xz}, \tau_{xy}\}^{(k)^T} \qquad (14)$$

$$\{e\}^{(k)} = \{e_x, e_y, \gamma_{yz}, \gamma_{xz}, \gamma_{xy}\}^{(k)^T} \qquad (15)$$

The reduced-transformed material constants $[\bar{C}]$ and transformed loss factors $[\bar{\eta}]$ are defined in Appendix D.

D. Strain Energy and Kinetic Energy

The bending strain energies per unit area of the N-layered plate are defined as

$$U_B = \frac{1}{2}\int_A \left[\sum_{k=1}^{N} \int_{z_{k-1}}^{z_k} \left(\sigma_x^{(k)} e_x^{(k)} + \sigma_y^{(k)} e_y^{(k)} + \tau_{xy}^{(k)} \gamma_{xy}^{(k)} \right) \mathrm{d}z \right] \mathrm{d}A \qquad (16)$$

and the shear strain energies per unit area of the N-layered plate are defined as

$$U_S = \frac{1}{2}\int_A \left[\sum_{k=1}^{N} \int_{z_{k-1}}^{z_k} \left(\tau_{xz}^{(k)} \gamma_{xz}^{(k)} + \tau_{yz}^{(k)} \gamma_{yz}^{(k)} \right) \mathrm{d}z \right] \mathrm{d}A \qquad (17)$$

The kinetic energy per unit area of the N-layered plate is given by

$$T = \frac{1}{2}\int_A \left\{ \sum_{k=1}^{N} \int_{z_{k-1}}^{z_k} \rho^{(k)} \left[\left(\frac{\partial u^{(k)}}{\partial t} \right)^2 + \left(\frac{\partial v^{(k)}}{\partial t} \right)^2 + \left(\frac{\partial w^{(k)}}{\partial t} \right)^2 \right] \mathrm{d}z \right\} \mathrm{d}A \qquad (18)$$

The stress resultants are defined as follows:

$$\begin{bmatrix} N_x & N_y & N_{xy} \\ M_x & M_y & M_{xy} \end{bmatrix} = \sum_{k=1}^{N} \int_{z_{k-1}}^{z_k} \begin{Bmatrix} 1 \\ z \end{Bmatrix} \begin{bmatrix} \sigma_x^{(k)} & \sigma_y^{(k)} & \tau_{xy}^{(k)} \end{bmatrix} \mathrm{d}z \quad (19)$$

$$\begin{bmatrix} P_{x1} & & P_{xy1} \\ P_{x2} & & P_{xy2} \\ & P_{y1} & P_{xy3} \\ & P_{y2} & P_{xy4} \end{bmatrix} = \sum_{k=1}^{N} \int_{z_{k-1}}^{z_k} \begin{Bmatrix} h_{11}^{(k)} \\ h_{12}^{(k)} \\ h_{21}^{(k)} \\ h_{22}^{(k)} \end{Bmatrix} \begin{bmatrix} \sigma_x^{(k)} & \sigma_y^{(k)} & \tau_{xy}^{(k)} \end{bmatrix} \mathrm{d}z \quad (20)$$

$$\begin{bmatrix} R_{x1} & \\ R_{x2} & \\ & R_{y1} \\ & R_{y2} \end{bmatrix} = \sum_{k=1}^{N} \int_{z_{k-1}}^{z_k} \begin{Bmatrix} h_{11,z}^{(k)} \\ h_{12,z}^{(k)} \\ h_{21,z}^{(k)} \\ h_{22,z}^{(k)} \end{Bmatrix} \begin{bmatrix} \tau_{xz}^{(k)} & \tau_{yz}^{(k)} \end{bmatrix} \mathrm{d}z \quad (21)$$

After the integration through the thickness is performed, the bending strain energy is written as

$$U_B = \frac{1}{2} \int_A \{\bar{\varepsilon}\}^T [T_B]^T [\hat{D}_B][T_B]\{\bar{\varepsilon}\} \, \mathrm{d}A \quad (22)$$

where the $\lfloor \hat{D}_B \rfloor$ is defined as

$$\lfloor \hat{D}_B \rfloor = [D_B] + i\left[D_B^d\right] \quad (23)$$

$$[D_B] = \begin{bmatrix} [A] & -[B] & [Q] \\ -[B] & [D] & -[E] \\ [Q]^T & -[E]^T & [G] \end{bmatrix}$$

$$\left[D_B^d\right] = \begin{bmatrix} [A_d] & -[B_d] & [Q_d] \\ -[B_d] & [D_d] & -[E_d] \\ [Q_d]^T & -[E_d]^T & [G_d] \end{bmatrix} \quad (24)$$

The shear strain energy is written as

$$U_S = \frac{1}{2} \int_A \{\bar{\gamma}\}^T [T_S]^T [\hat{D}_S][T_S]\{\bar{\gamma}\} \, \mathrm{d}A \quad (25)$$

where the $\lfloor \hat{D}_S \rfloor$ is defined as

$$\lfloor \hat{D}_S \rfloor = [F] + i[F_d] \quad (26)$$

The resultant elastic material constants (A, B, D, Q, E, G, F) and the damping constants A_d, B_d, D_d, Q_d, E_d, G_d, and F_d are defined in Appendix B. The velocity vector using the interdependent kinematic relation (5) is defined as

$$\boldsymbol{V} = [T_\rho]\boldsymbol{V}_R \quad (27)$$

where $\lfloor T_\rho \rfloor$ is defined in Appendix C and the reduced velocity vector $\boldsymbol{V}_R$ is defined as

$$\boldsymbol{V}_R = \left\{ \dot{u}_0, \dot{v}_0, \dot{w}_0, \frac{\partial \dot{w}_0}{\partial x}, \frac{\partial \dot{w}_0}{\partial y} \right\}^T \quad (28)$$

and the effective inertia constants are defined as

$$[Z_\rho] = \begin{bmatrix} I_0 & 0 & 0 & -I_1 & 0 & H_0^{11} & H_0^{12} \\ 0 & I_0 & 0 & 0 & -I_1 & H_0^{21} & H_0^{22} \\ 0 & 0 & I_0 & 0 & 0 & 0 & 0 \\ -I_1 & 0 & 0 & I_2 & 0 & -H_1^{11} & -H_1^{12} \\ 0 & -I_1 & 0 & 0 & I_2 & -H_1^{21} & -H_1^{22} \\ H_0^{11} & H_0^{21} & 0 & -H_1^{11} & -H_1^{21} & \left(H_{11}^2 + H_{21}^2\right) & \left(H_2^{12} + H_2^{21}\right) \\ H_0^{12} & H_0^{22} & 0 & -H_1^{12} & -H_1^{22} & \left(H_2^{12} + H_2^{21}\right) & \left(H_{12}^2 + H_{22}^2\right) \end{bmatrix} \quad (29)$$

where I_0, I_1, I_2, H_0^{11}, H_0^{12}, H_0^{21}, H_0^{22}, H_1^{11}, H_1^{12}, H_1^{21}, H_1^{22}, H_{11}^2, H_{12}^2, H_{21}^2, H_{22}^2, H_2^{12}, and H_2^{21} are defined in Appendix B. The kinetic energy is written as

$$T = \frac{1}{2} \int_A \{V_R\}^T [T_\rho]^T [Z_\rho][T_\rho]\{V_R\} \, \mathrm{d}A \quad (30)$$

III. Three-Node Triangular Element

A three-node triangular element based on the improved higher-order zig-zag displacement field (1) is developed (Fig. 1). The in-plane displacements u_0 and v_0 are linearly interpolated as

$$u_0 = \sum_{i=1}^{3} n_i u_0^i, \qquad v_0 = \sum_{i=1}^{3} n_i v_0^i \quad (31)$$

and the shape function n_i is defined as

$$n_i = \zeta_i \quad (32)$$

where ζ_i are the areal coordinate systems in a triangular element (Fig. 1). The transverse displacement w_0, which is C^1 continuous subparametric, is interpolated using the shape functions suggested by Specht[17] as

$$w_0 = \sum_{i=1}^{3} \left(q_i w_0^i + g_i \theta_x^i + h_i \theta_y^i \right) \quad (33)$$

where

$$\theta_x^i = \left(\frac{\partial w_0}{\partial y} \right)_i, \qquad \theta_y^i = -\left(\frac{\partial w_0}{\partial x} \right)_i \quad (34)$$

and q_i, g_i, and h_i are defined by Specht[17] as

$$\begin{aligned} q_i &= P_i - P_{i+3} + P_{k+3} + 2(P_{i+6} - P_{k+6}) \\ g_i &= b_j(P_{k+6} - P_{k+3}) + b_k P_{i+6} \\ h_i &= c_j(P_{k+6} - P_{k+3}) + c_k P_{i+6} \end{aligned} \quad (35)$$

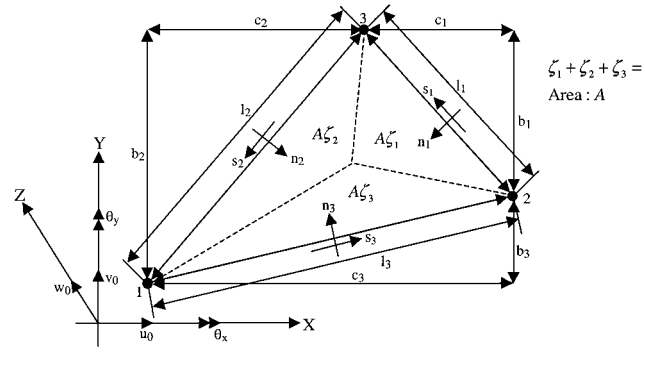

Fig. 1 Geometry and coordinate system for triangular element.

Here, i, j, and k are the cyclic permutations of 1, 2, and 3 and

$$b_i = y_j - y_k, \qquad c_i = x_k - x_j \tag{36}$$

where x_i and y_i are the coordinates of each three vertices of the triangular element. P_i are defined by Specht[17] as

$$\begin{aligned}\{P\} = \{&\zeta_1, \zeta_2, \zeta_3, \zeta_1\zeta_2, \zeta_2\zeta_3, \zeta_3\zeta_1, \zeta_1^2\zeta_2 \\ &+ \tfrac{1}{2}\zeta_1\zeta_2\zeta_3[3(1-\mu_3)\zeta_1 - (1+3\mu_3)\zeta_2 + (1+3\mu_3)\zeta_3]\zeta_2^2\zeta_3 \\ &+ \tfrac{1}{2}\zeta_1\zeta_2\zeta_3[3(1-\mu_1)\zeta_2 - (1+3\mu_1)\zeta_3 + (1+3\mu_1)\zeta_1]\zeta_3^2\zeta_1 \\ &+ \tfrac{1}{2}\zeta_1\zeta_2\zeta_3[3(1-\mu_2)\zeta_3 - (1+3\mu_2)\zeta_1 + (1+3\mu_2)\zeta_2]\}\end{aligned} \tag{37}$$

where

$$\mu_1 = \frac{l_3^2 - l_2^2}{l_1^2}, \qquad \mu_2 = \frac{l_1^2 - l_3^2}{l_2^2}, \qquad \mu_3 = \frac{l_2^2 - l_1^2}{l_3^2} \tag{38}$$

where l_1, l_2, and l_3 are the lengths of the three sides of the triangle (see Fig. 1). The membrane-bending and transverse shear strain vectors with respect to the areal coordinate system are defined as

$$\{\bar{\varepsilon}\} = [N_B]\{d_e\} \tag{39}$$

$$\{\bar{\gamma}\} = [N_S]\{d_e\} \tag{40}$$

where the shape functions N_B and N_S are defined in Appendix E. The elemental degrees of freedom $\{d_e\}$ are defined as

$$\{d_e\} = \{\{d_e\}_1, \{d_e\}_2, \{d_e\}_3\} \tag{41}$$

where

$$\{d_e\}_i = \{u_0^i, v_0^i, w_0^i, \theta_x^i, \theta_y^i\}, \qquad i = 1, 2, 3$$

Substituting Eqs. (39) and (40) into Eqs. (22) and (25) leads to the stiffness matrices for the membrane-bending and transverse shear part as

$$[K_B] = \int_0^1 \int_0^{1-\zeta_1} [N_B]^T [T_B]^T [D_B][T_B][N_B] 2A \, \mathrm{d}\zeta_2 \, \mathrm{d}\zeta_1 \tag{42}$$

$$[K_S] = \int_0^1 \int_0^{1-\zeta_1} [N_S]^T [T_S]^T [D_S][T_S][N_S] 2A \, \mathrm{d}\zeta_2 \, \mathrm{d}\zeta_1 \tag{43}$$

$$\left[K_B^d\right] = \int_0^1 \int_0^{1-\zeta_1} [N_B]^T [T_B]^T \left[D_B^d\right][T_B][N_B] 2A \, \mathrm{d}\zeta_2 \, \mathrm{d}\zeta_1 \tag{44}$$

$$\left[K_S^d\right] = \int_0^1 \int_0^{1-\zeta_1} [N_S]^T [T_S]^T \left[D_S^d\right][T_S][N_S] 2A \, \mathrm{d}\zeta_2 \, \mathrm{d}\zeta_1 \tag{45}$$

where sixth-order single-summation Gauss quadrature numerical integration for triangles is used. The stiffness and damping matrices are defined as

$$[K] = [K_B] + [K_S], \qquad [K_D] = \lfloor K_B^d \rfloor + \lfloor K_S^d \rfloor \tag{46}$$

The velocity vector is defined as

$$\boldsymbol{V}_R = [N_\rho]\{\dot{d}_e\} \tag{47}$$

where $\lfloor N_\rho \rfloor$ is defined in Appendix E. Substituting Eq. (47) into Eq. (30) leads to the consistent mass matrix

$$[M] = \int_0^1 \int_0^{1-\zeta_1} [N_\rho]^T [T_\rho]^T [Z_\rho][T_\rho][N_\rho] 2A \, \mathrm{d}\zeta_2 \, \mathrm{d}\zeta_1 \tag{48}$$

where the integration is conducted numerically with sixth-order single-summation Gauss quadrature.

IV. Governing Equations

The governing differential equations of motion for laminated plates incorporating the improved higher-order zig-zag theory are derived using Hamilton's principle, as follows:

$$[M]\{\ddot{d}\} + ([K] + i[K_D])\{d\} = \{0\} \tag{49}$$

The eigenvalue problem Eq. (49) is solved to find the natural frequencies and modal loss factors by the modal strain energy method (MSE) with the subspace iteration method. The modal loss factor of the nth mode is given by

$$\eta_n = \frac{\{\chi_n\}^T [K_D]\{\chi_n\}}{\{\chi_n\}^T [K]\{\chi_n\}} \tag{50}$$

where the nth normal mode $\{\chi_n\}$ is found by solving the undamped free vibration problem.

V. Numerical Results

The natural frequencies and modal loss factors of various cantilevered rectangular laminated plates with an embedded damping layer are calculated. Various fiber orientations, border materials, and damping layers are investigated. Current calculated results are compared to the experimental results and analytical (MSC/NASTRAN) results in which the face sheets are modeled with plate elements (CTRIA) and the damping core is modeled with solid elements (CPENTA). The plate nodes are to be offset to one surface of the plate, coincident with the corner nodes of the adjoining solid elements. The offset plate elements have coupling between stretching and bending deformations.

The cantilevered laminated rectangular plates consisted of graphite/epoxy (GE) face sheets and a damping core layer. See Fig. 2 for the components of the damped plates and Fig. 3 for the geometric definition of the damping core layer. The material properties for GE used for the face sheets are as follows:

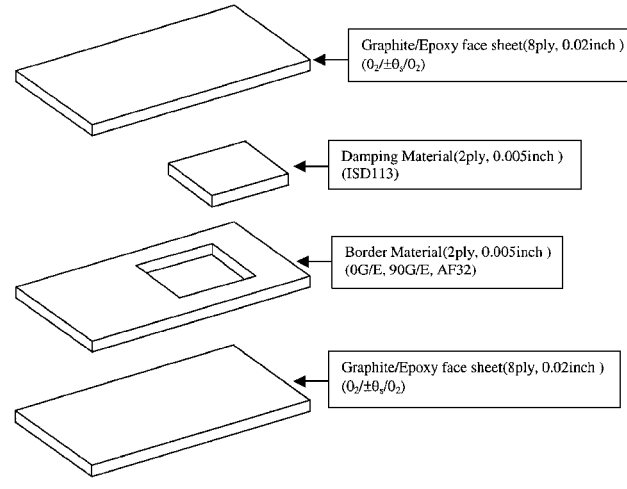

Fig. 2 Damped plate components.

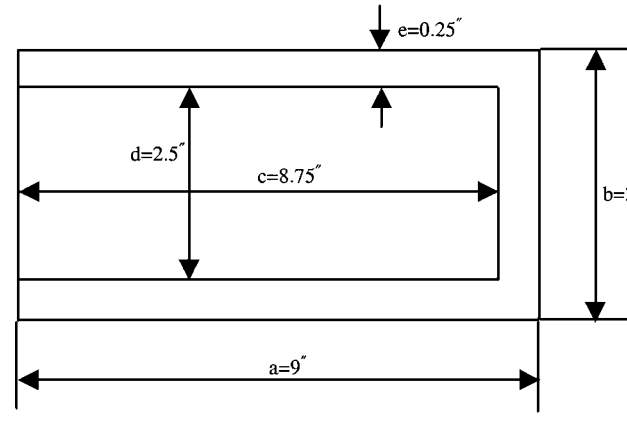

Fig. 3 Geometry of central core layer.

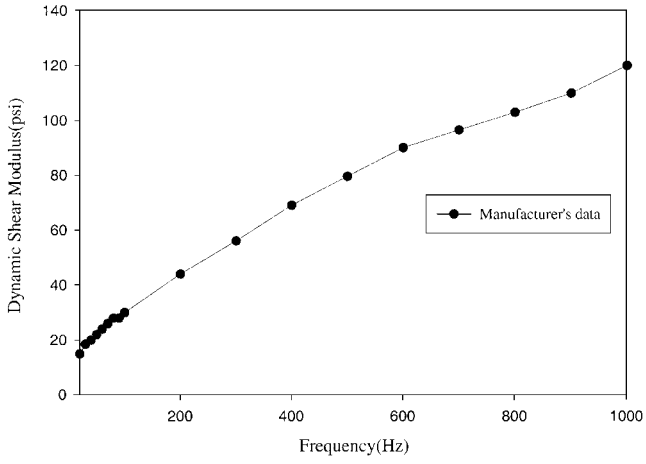

Shear modulus

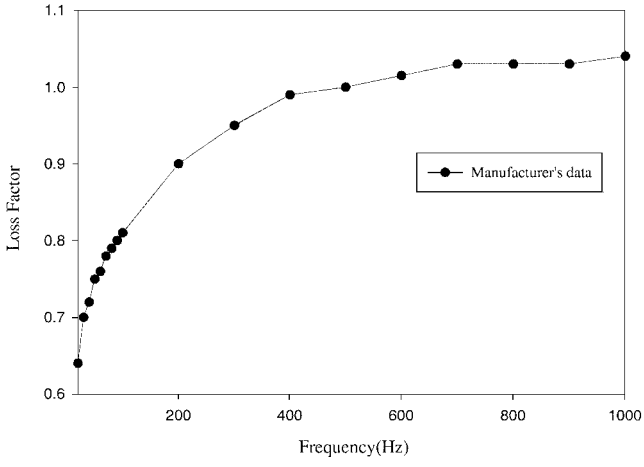

Shear loss factor

Fig. 4 Mechanical properties of ISD113 viscoelastic polymer at 68°F (20°C).

$E_L = 2 \times 10^7$ psi (138 GPa), $E_T = 1.4 \times 10^6$ psi (9.7 GPa), $G_{LT} = 8 \times 10^5$ psi (5.5 GPa), $G_{TT} = 5 \times 10^5$ psi (3.5 GPa), $\nu_{LT} = 0.3$, $\rho = 1.485 \times 10^{-4}$ lbf-s^2/in.^{4} (1587 kg/m^3), and $h_{\text{ply}} = 0.0025$ in. (0.0635 mm). The loss factors used for the GE lamina are found by correlating the experimental results of an undamped GE plate to the finite element solutions by the MSE:

$$\eta_L = \eta_T = 0.0026, \qquad \eta_{LT} = \eta_{TT} = 0.026$$

The 3M ISD113 is used for the central damping core in this study, and the shear modulus and loss factor for ISD113 are found in the manufacturer supplied nomogram (Fig. 4) for the desired frequency at the room temperature (68°F) (20°C): $\rho_{\text{ISD113}} = 0.917 \times 10^{-4}$ lbf-s^2/in.^{4} (980 kg/m^3). 3M AF32 is used for the central core border material, and the shear modulus and loss factor for AF32 are found in the manufacturer supplied nomogram (Fig. 5) for the desired frequency at the room temperature (68°F) (20°C): $\rho_{\text{AF32}} = 0.989 \times 10^{-4}$ lbf-s^2/in.^{4} (1057 kg/m^3). Figure 6 shows the mesh representation used for the finite element analysis. In Table 1, a comparison of the required nodes and DOF for the current model and MSC/NASTRAN model are presented.

The natural frequencies and modal loss factors are calculated by the MSE and compared to the experimental results and NASTRAN results with the MSE.

Analytical results using the present three-node zig-zag triangular element (THZ3R) are presented in Tables 2–8 along with experimentally measured results and analytical results using MSC/NASTRAN. The vibration frequencies and loss factors of the first bending (1B), second bending (2B), and first torsion (1T) modes of the cantilevered composite plates are presented. The current results show good agreement with the experimentally measured natural frequencies and modal loss factors for various fiber angles and border materials. MSC/NASTRAN results with plate–solid elements show good

Table 1 Details of finite element scheme

Parameter	Present (THZ3R)	MSC/NASTRAN (CTRIA/CPENTA)
Elements	1584	4752
Nodes	855	1710
DOF	4275	10260

Table 2 Calculated and experimental frequencies of cantilevered undamped plate [$0_2/\pm 15_s/0_2$ deg]| [90 deg]| [$0_2/\pm 15_s/0_2$ deg]

	Present ω, Hz			Experiment	
Mode	(2 × 6)	(4 × 12)	(6 × 18)	ω, Hz	η
1B	32.18	32.05	32.01	31.21	0.003
1T	106.88	98.54	96.84	100.0	0.012
2B	208.46	202.03	200.68	194.6	0.004

Table 3 Frequencies and loss factors of cantilevered damped plate [$0_2/\pm 15_s/0_2$ deg]| [ISD 113 − 0 deg GE]| [$0_2/\pm 15_s/0_2$ deg]

	ω, Hz			η		
Mode	Experiment	Present	NASTRAN	Experiment	Present	NASTRAN
1B	28.4	29.94	30.18	0.014	0.016	0.011
1T	92.5	93.58	94.07	0.017	0.024	0.011
2B	163.5	157.48	159.43	0.059	0.065	0.059

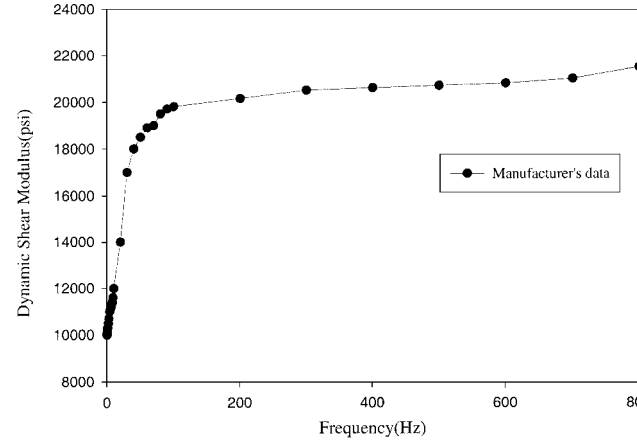

Shear modulus

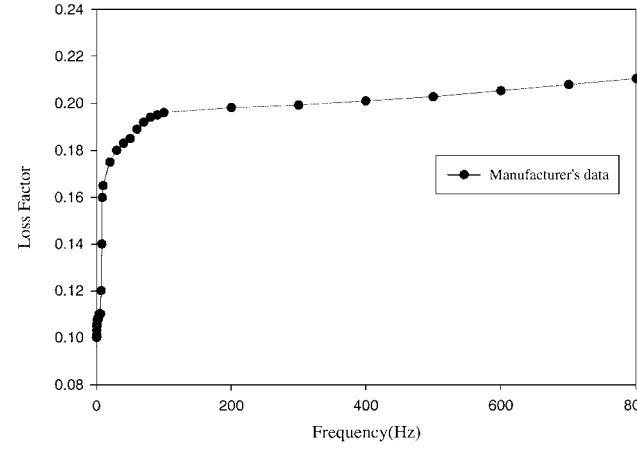

Shear loss factor

Fig. 5 Mechanical properties of AF-32 adhesive at 68°F.

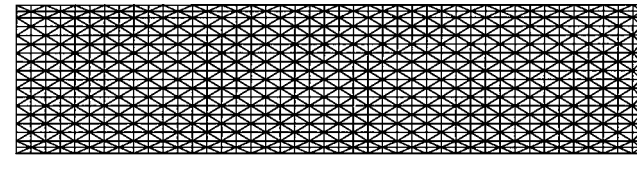

Fig. 6 Finite element mesh representation.

Table 4 Frequencies and loss factors of cantilevered damped plate [$0_2/\pm 15_s/0_2$ deg] [ISD 113 − 90 deg GE] [$0_2/\pm 15_s/0_2$ deg]

	ω, Hz			η		
Mode	Experiment	Present	NASTRAN	Experiment	Present	NASTRAN
1B	27.97	29.93	30.18	0.018	0.016	0.011
1T	83.23	93.56	94.05	0.022	0.024	0.011
2B	163.7	157.43	159.37	0.063	0.065	0.059

Table 5 Frequencies and loss factors of cantilevered damped plate [$0_2/\pm 15_s/0_2$ deg] [ISD 113 − AF 32] [$0_2/\pm 15_s/0_2$ deg]

	ω, Hz			η		
Mode	Experiment	Present	NASTRAN	Experiment	Present	NASTRAN
1B	27.46	29.82	30.05	0.028	0.02	0.016
1T	87.22	93.03	93.44	0.035	0.029	0.016
2B	161.4	155.04	156.55	0.077	0.077	0.071

Table 6 Frequencies and loss factors of cantilevered damped plate [$0_2/\pm 45_s/0_2$ deg] [ISD 113 − 0 deg GE] [$0_2/\pm 45_s/0_2$ deg]

	ω, Hz			η		
Mode	Experiment	Present	NASTRAN	Experiment	Present	NASTRAN
1B	24.83	26.32	26.51	0.008	0.007	0.003
1T	124.6	121.44	122.07	0.015	0.029	0.021
2B	147.9	148.32	150.05	0.037	0.033	0.027

Table 7 Frequencies and loss factors of cantilevered damped plate [$0_2/\pm 45_s/0_2$ deg] [ISD 113 − 90 deg GE] [$0_2/\pm 45_s/0_2$ deg]

	ω, Hz			η		
Mode	Experiment	Present	NASTRAN	Experiment	Present	NASTRAN
1B	24.44	26.32	26.51	0.007	0.008	0.003
1T	128.2	121.39	122.04	0.012	0.029	0.021
2B	145.3	148.25	149.99	0.05	0.033	0.027

Table 8 Frequencies and loss factors of cantilevered damped plate [$0_2/\pm 45_s/0_2$ deg] [ISD 113 − *AF*32] [$0_2/\pm 45_s/0_2$ deg]

	ω, Hz			η		
Mode	Experiment	Present	NASTRAN	Experiment	Present	NASTRAN
1B	23.93	26.27	26.44	0.017	0.01	0.006
1T	119.5	120.02	120.5	0.033	0.035	0.028
2B	144.0	146.49	147.67	0.052	0.043	0.038

agreement in natural frequencies but larger errors in the modal loss factors because the plate–solid elements do not accurately represent the shear deformations in the damping core. The accuracy of the MSC/NASTRAN plate–solid–plate model can be improved by adding more solid elements through the core thickness but at an enormous increase in computational cost.

A comparison of Tables 2 and 5 reveals that embedding an ISD 113/AF-32 damping core in a composite laminate can greatly increase the damping loss factor over an undamped plate. These increases for the first three modes are 9.3, 2.9, and 19.3 times, respectively. A comparison of Tables 3, 4, and 5 for a fiber orientation of 15 deg and Tables 6, 7, and 8 for a fiber orientation of 45 deg reveals that an AF32-border material produces higher modal loss factors than a unidirectional GE border because AF32 itself has significant damping capability. Further examination of Tables 3–8 reveal that the bending frequencies and corresponding modal loss factors for the fiber angle 15 deg are greater than for the fiber angle 45 deg, whereas the torsional frequencies and loss factors for a fiber angle of 45 deg are higher than the fiber angle of 15 deg.

The frequency and corresponding modal loss factor variations of symmetric laminated undamped $[\theta_4/-\theta_4]$ $[90_2$ deg$]$ $[-\theta_4/\theta_4]$ and damped $[\theta_4/-\theta_4]$ [ISD 113] $[-\theta_4/\theta_4]$ plates as a function of fiber angles are depicted in Figs. 7 and 8. The undamped bending

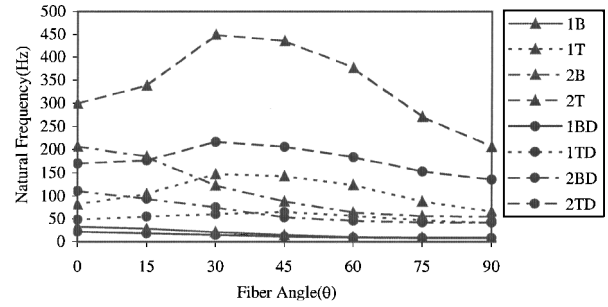

Fig. 7 Frequencies of symmetric laminated undamped $[\theta_4/-\theta_4]$ $[90_2$ deg$]$ $[-\theta_4/\theta_4]$ and damped $[\theta_4/-\theta_4]$ [ISD 113] $[-\theta_4/\theta_4]$ cantilever plates.

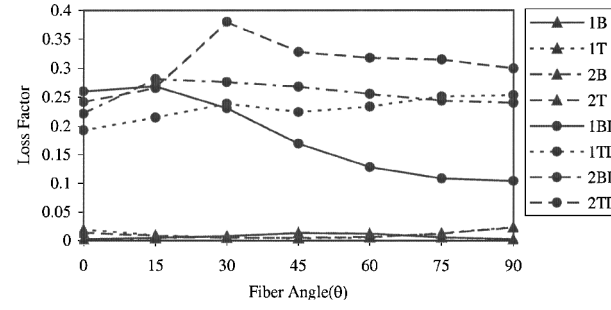

Fig. 8 Loss factors of symmetric laminated undamped $[\theta_4/-\theta_4]$ $[90_2$ deg$]$ $[-\theta_4/\theta_4]$ and damped $[\theta_4/-\theta_4]$ [ISD 113] $[-\theta_4/\theta_4]$ cantilever plates.

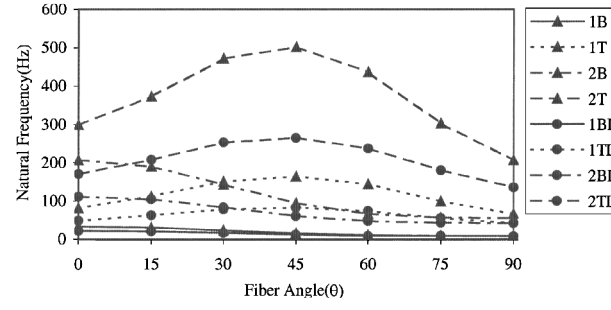

Fig. 9 Frequencies of antisymmetric laminated undamped $[\theta_4/-\theta_4]$ $[90_2$ deg$]$ $[\theta_4/-\theta_4]$ and damped $[\theta_4/-\theta_4]$ [ISD 113] $[\theta_4/-\theta_4]$ cantilever plates.

frequencies ω_{1B} and ω_{2B} and damped bending frequencies ω_{1BD} and ω_{2BD} are decreasing as fiber angle θ is increasing because the axial bending stiffness is decreasing. The undamped torsional frequencies ω_{1T} and ω_{2T} have maximums at 30 deg, and the first damped torsional frequency ω_{1TD} reaches a maximum at 45 deg. The second damped torsional frequency ω_{2TD} has its maximum at 30 deg because the shear stiffness has maximum value at those angles. The undamped bending loss factors η_{1B} and η_{2B} have maximums at 45 deg, whereas undamped torsional loss factors η_{1T} and η_{2T} have minimums at 45 deg because the energy dissipating shear deformation is at a minimum for torsinal modes and a maximum for bending modes at 45 deg. The damped bending loss factors η_{1BD} and η_{2BD} have maximums at 15 deg and decrease as the fiber angle increase beyond 15 deg. The first damped torsional loss factor η_{1TD} has a local maximum at 30 deg, a local minimum at 45 deg, and tends to increase as fiber angle is increasing. The second damped loss factor η_{2TD} has a maximum at 30 deg. Figures 9 and 10 show the frequency and modal loss factor variations of antisymmetric laminated undamped $[\theta_4/-\theta_4][90_2$ deg$][\theta_4/-\theta_4]$ and damped $[\theta_4/-\theta_4]$ [ISD 113] $[\theta_4/-\theta_4]$ plates as a function of fiber angles, respectively. The undamped bending frequencies ω_{1B} and ω_{2B} and damped bending frequencies ω_{1BD} and ω_{2BD} are decreasing as fiber angle θ is increasing. The undamped torsional frequencies ω_{1T} and ω_{2T} and damped torsional frequencies ω_{1TD} and ω_{2TD} reach maximums at 45 deg. The first undamped bending loss factor η_{1B} has maximum at 60 deg,

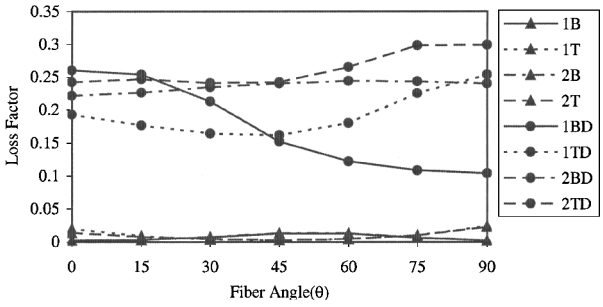

Fig. 10 Loss factors of antisymmetric laminated undamped $[\theta_4/-\theta_4]$ $[90_2$ deg$]$ $[\theta_4/-\theta_4]$ and damped $[\theta_4/-\theta_4]$ [ISD 113] $[\theta_4/-\theta_4]$ cantilever plates.

and the second undamped bending loss factor η_{2B} has a maximum at 45 deg. The undamped torsional loss factors η_{1T} and η_{2T} have minimums at 45 deg. The first damped bending loss factor η_{1BD} is decreasing as the fiber angle is increasing. The second damped bending loss factor η_{2BD} has maximum at 60 deg. The first torsioanl damped loss factor η_{1TD} has minimum at 45 deg. The second torsional damped loss factor η_{2TD} has minimum at 30 deg.

VI. Conclusions

A three-node zig-zag triangular element was developed based on the improved layerwise zig-zag theory and the interdependent kinematic relations. The zig-zag triangular element is capable of analyzing the behavior of laminated structures having an arbitrary ply thickness variation, extreme ply rigidity differences, and ply damping. The triangular element is in close agreement with experimentally measured natural frequencies and modal loss factors for various fiber angles and border materials. This element is easy to implement and more accurate than using an assembly of plate and solid elements for analyzing damped laminated structures (MSC/NASTRAN).

Appendix A: Zig-Zag Displacement Coefficients

The coefficients in the refined higher-order zig-zag displacement field are defined as

$$f_1 = \left[\left(\sum_{i=1}^{N-1} b_{3i}\right)\left(\sum_{i=1}^{N-1} c_{2i}\right) - \left(2h + \sum_{i=1}^{N-1} a_{2i}\right)\left(3h^2 + \sum_{i=1}^{N-1} d_{3i}\right)\right] \Big/ D_e \tag{A1}$$

$$f_2 = \left[\left(\sum_{i=1}^{N-1} b_{3i}\right)\left(2h + \sum_{i=1}^{N-1} d_{2i}\right) - \left(\sum_{i=1}^{N-1} b_{2i}\right)\left(3h^2 + \sum_{i=1}^{N-1} d_{3i}\right)\right] \Big/ D_e \tag{A2}$$

$$f_3 = \left[\left(\sum_{i=1}^{N-1} c_{3i}\right)\left(2h + \sum_{i=1}^{N-1} a_{2i}\right) - \left(\sum_{i=1}^{N-1} c_{2i}\right)\left(3h^2 + \sum_{i=1}^{N-1} a_{3i}\right)\right] \Big/ D_e \tag{A3}$$

$$f_4 = \left[\left(\sum_{i=1}^{N-1} c_{3i}\right)\left(\sum_{i=1}^{N-1} b_{2i}\right) - \left(2h + \sum_{i=1}^{N-1} d_{2i}\right)\left(3h^2 + \sum_{i=1}^{N-1} a_{3i}\right)\right] \Big/ D_e \tag{A4}$$

$$D_e = \left[\left(3h^2 + \sum_{i=1}^{N-1} d_{3i}\right)\left(3h^2 + \sum_{i=1}^{N-1} a_{3i}\right) - \left(\sum_{i=1}^{N-1} c_{3i}\right)\left(\sum_{i=1}^{N-1} b_{3i}\right)\right] \tag{A5}$$

where h is the total thickness of the laminate. N is the number of layers in the laminate. Thus,

$$a_{2i} = \hat{a}_i\left(2z_i + \sum_{q=1}^{i-1} a_{2q}\right) + \hat{b}_i\left(\sum_{q=1}^{i-1} c_{2q}\right) \tag{A6}$$

$$a_{3i} = \hat{a}_i\left(3z_i^2 + \sum_{q=1}^{i-1} a_{3q}\right) + \hat{b}_i\left(\sum_{q=1}^{i-1} c_{3q}\right) \tag{A7}$$

$$b_{2i} = \hat{b}_i\left(2z_i + \sum_{q=1}^{i-1} d_{2q}\right) + \hat{a}_i\left(\sum_{q=1}^{i-1} b_{2q}\right) \tag{A8}$$

$$b_{3i} = \hat{b}_i\left(3z_i^2 + \sum_{q=1}^{i-1} d_{3q}\right) + \hat{a}_i\left(\sum_{q=1}^{i-1} b_{3q}\right) \tag{A9}$$

$$c_{2i} = \hat{c}_i\left(2z_i + \sum_{q=1}^{i-1} a_{2q}\right) + \hat{d}_i\left(\sum_{q=1}^{i-1} c_{2q}\right) \tag{A10}$$

$$c_{3i} = \hat{c}_i\left(3z_i^2 + \sum_{q=1}^{i-1} a_{3q}\right) + \hat{d}_i\left(\sum_{q=1}^{i-1} c_{3q}\right) \tag{A11}$$

$$d_{2i} = \hat{d}_i\left(2z_i + \sum_{q=1}^{i-1} d_{2q}\right) + \hat{c}_i\left(\sum_{q=1}^{i-1} b_{2q}\right) \tag{A12}$$

$$d_{3i} = \hat{d}_i\left(3z_i^2 + \sum_{q=1}^{i-1} d_{3q}\right) + \hat{c}_i\left(\sum_{q=1}^{i-1} b_{3q}\right) \tag{A13}$$

$$\hat{a}_i = \frac{\bar{C}_{44}^{i+1}\bar{C}_{55}^{i} - \bar{C}_{45}^{i+1}\bar{C}_{45}^{i}}{\Delta_{i+1}} - 1 \tag{A14}$$

$$\hat{b}_i = \frac{\bar{C}_{44}^{i+1}\bar{C}_{45}^{i} - \bar{C}_{45}^{i+1}\bar{C}_{44}^{i}}{\Delta_{i+1}} \tag{A15}$$

$$\hat{c}_i = \frac{\bar{C}_{55}^{i+1}\bar{C}_{45}^{i} - \bar{C}_{45}^{i+1}\bar{C}_{55}^{i}}{\Delta_{i+1}} \tag{A16}$$

$$\hat{d}_i = \frac{\bar{C}_{55}^{i+1}\bar{C}_{44}^{i} - \bar{C}_{45}^{i+1}\bar{C}_{45}^{i}}{\Delta_{i+1}} - 1 \tag{A17}$$

$$\Delta_{i+1} = \bar{C}_{55}^{i+1}\bar{C}_{44}^{i+1} - \left(\bar{C}_{45}^{i+1}\right)^2 \tag{A18}$$

Appendix B: Material Constitutive Constants

The resultant elastic material constants are defined as

$$[A, B, D] = \sum_{k=1}^{N} \int_{z_{k-1}}^{z_k} [1, z, z^2][\bar{C}_B]^{(k)}\,\mathrm{d}z \tag{B1}$$

$$[Q, E] = \sum_{k=1}^{N} \int_{z_{k-1}}^{z_k} [1, z][\bar{C}_B]^{(k)}[Z]\,\mathrm{d}z \tag{B2}$$

$$[G] = \sum_{k=1}^{N} \int_{z_{k-1}}^{z_k} [Z]^T[\bar{C}_B]^{(k)}[Z]\,\mathrm{d}z \tag{B3}$$

$$[F] = \sum_{k=1}^{N} \int_{z_{k-1}}^{z_k} [ZZ]^T[\bar{C}_S]^{(k)}[ZZ]\,\mathrm{d}z \tag{B4}$$

where $[\bar{C}_B]^{(k)}$, $[\bar{C}_S]^{(k)}$, $[Z]$, and $[ZZ]$ are defined as

$$[\bar{C}_B]^{(k)} = \begin{bmatrix} \bar{C}_{11} & \bar{C}_{12} & \bar{C}_{16} \\ \bar{C}_{12} & \bar{C}_{22} & \bar{C}_{26} \\ \bar{C}_{16} & \bar{C}_{26} & \bar{C}_{66} \end{bmatrix}^{(k)} \tag{B5}$$

$$[\bar{C}_S]^{(k)} = \begin{bmatrix} \bar{C}_{44} & \bar{C}_{45} \\ \bar{C}_{45} & \bar{C}_{55} \end{bmatrix}^{(k)} \tag{B6}$$

$$[Z] = \begin{bmatrix} h_{11}^{(k)} & h_{12}^{(k)} & 0 & 0 \\ 0 & 0 & h_{21}^{(k)} & h_{22}^{(k)} \\ h_{21}^{(k)} & h_{22}^{(k)} & h_{11}^{(k)} & h_{12}^{(k)} \end{bmatrix} \tag{B7}$$

$$[ZZ] = \begin{bmatrix} h_{21,z}^{(k)} & h_{22,z}^{(k)} \\ h_{11,z}^{(k)} & h_{12,z}^{(k)} \end{bmatrix} \tag{B8}$$

The resultant damping material constants (A_d, B_d, D_d, Q_d, E_d, G_d, and F_d) are calculated by substituting $[\bar{C}_B]^{(k)}[\bar{\eta}_B]^{(k)}$ and $[\bar{C}_S]^{(k)}[\bar{\eta}_S]^{(k)}$ for $[\bar{C}_B]^{(k)}$ and $[\bar{C}_S]^{(k)}$, respectively, in Eqs. (B1–B4), and $[\bar{\eta}_B]^{(k)}$ and $[\bar{\eta}_S]^{(k)}$ are defined as

$$[\bar{\eta}_B]^{(k)} = \begin{bmatrix} \bar{\eta}_{11} & \bar{\eta}_{12} & \bar{\eta}_{16} \\ \bar{\eta}_{21} & \bar{\eta}_{22} & \bar{\eta}_{26} \\ \bar{\eta}_{61} & \bar{\eta}_{62} & \bar{\eta}_{66} \end{bmatrix}^{(k)} \tag{B9}$$

$$[\bar{\eta}_S]^{(k)} = \begin{bmatrix} \bar{\eta}_{44} & \bar{\eta}_{45} \\ \bar{\eta}_{54} & \bar{\eta}_{55} \end{bmatrix}^{(k)} \tag{B10}$$

The resultant inertia constants are defined as

$$(I_0, I_1, I_2) = \sum_{k=1}^{N} \int_{z_{k-1}}^{z_k} \rho^{(k)}(1, z, z^2)\, \mathrm{d}z \tag{B11}$$

$$\left(H_0^{11}, H_0^{12}, H_0^{21}, H_0^{22}\right) = \sum_{k=1}^{N} \int_{z_{k-1}}^{z_k} \rho^{(k)} \left(h_{11}^{(k)}, h_{12}^{(k)}, h_{21}^{(k)}, h_{22}^{(k)}\right) \mathrm{d}z \tag{B12}$$

$$\left(H_1^{11}, H_1^{12}, H_1^{21}, H_1^{22}\right) = \sum_{k=1}^{N} \int_{z_{k-1}}^{z_k} \rho^{(k)} z \left(h_{11}^{(k)}, h_{12}^{(k)}, h_{21}^{(k)}, h_{22}^{(k)}\right) \mathrm{d}z \tag{B13}$$

$$\left(H_{11}^2, H_{12}^2, H_{21}^2, H_{22}^2\right) = \sum_{k=1}^{N} \int_{z_{k-1}}^{z_k} \rho^{(k)} \left(h_{11}^{(k)2}, h_{12}^{(k)2}, h_{21}^{(k)2}, h_{22}^{(k)2}\right) \mathrm{d}z \tag{B14}$$

$$\left(H_2^{12}, H_2^{21}\right) = \sum_{k=1}^{N} \int_{z_{k-1}}^{z_k} \rho^{(k)} \left(h_{11}^{(k)} h_{12}^{(k)}, h_{21}^{(k)} h_{22}^{(k)}\right) \mathrm{d}z \tag{B15}$$

Appendix C: Interdependent Kinematic Transformation Matrices

The transformation matrices are

$$[T_B] = \begin{bmatrix} 1 & 0 & 0 & 0 & 0 & 0 & 0 \\ 0 & 0 & 0 & 1 & 0 & 0 & 0 \\ 0 & 1 & 1 & 0 & 0 & 0 & 0 \\ 0 & 0 & 0 & 0 & 1 & 0 & 0 \\ 0 & 0 & 0 & 0 & 0 & 1 & 0 \\ 0 & 0 & 0 & 0 & 0 & 0 & 2 \\ -c_x^1 & c_x^3 & 0 & 0 & c_x^2 & 0 & -c_x^4 \\ c_y^1 & -c_y^3 & 0 & 0 & -c_y^2 & 0 & c_y^4 \\ 0 & 0 & -c_x^1 & c_x^3 & 0 & -c_x^4 & c_x^2 \\ 0 & 0 & c_y^1 & -c_y^3 & 0 & c_y^4 & -c_y^2 \end{bmatrix} \tag{C1}$$

$$[T_S] = \begin{bmatrix} -c_x^1 & c_x^3 & c_x^2 & -c_x^4 \\ c_y^1 & -c_y^3 & -c_y^2 & c_y^4 \end{bmatrix} \tag{C2}$$

$$[T_\rho] = \begin{bmatrix} 1 & 0 & 0 & 0 & 0 \\ 0 & 1 & 0 & 0 & 0 \\ 0 & 0 & 1 & 0 & 0 \\ 0 & 0 & 0 & 1 & 0 \\ 0 & 0 & 0 & 0 & 1 \\ -c_x^1 & c_x^3 & 0 & c_x^2 & -c_x^4 \\ c_y^1 & -c_y^3 & 0 & -c_y^2 & c_y^4 \end{bmatrix} \tag{C3}$$

where c_x^1, c_x^2, c_x^3, and c_x^4 and c_y^1, c_y^2, c_y^3, and c_y^4 are defined in Eq. (6).

Appendix D: Complex Constitutive Relations for Orthotropic Materials

The reduced-transformed elastic orthotropic material constants for kth layer are defined as

$$[\bar{C}]^{(k)} = \begin{bmatrix} \bar{C}_{11} & \bar{C}_{12} & 0 & 0 & \bar{C}_{16} \\ \bar{C}_{12} & \bar{C}_{22} & 0 & 0 & \bar{C}_{26} \\ 0 & 0 & \bar{C}_{44} & \bar{C}_{45} & 0 \\ 0 & 0 & \bar{C}_{45} & \bar{C}_{55} & 0 \\ \bar{C}_{16} & \bar{C}_{26} & 0 & 0 & \bar{C}_{66} \end{bmatrix}^{(k)} \tag{D1}$$

where

$$[\bar{C}]^{(k)} = [R(\theta_k)][C]^{(k)}[R(\theta_k)]^T \tag{D2}$$

and the elastic orthotropic material constants in principal axes are defined as

$$[C]^{(k)} = \begin{bmatrix} C_{11} & C_{12} & 0 & 0 & 0 \\ C_{12} & C_{22} & 0 & 0 & 0 \\ 0 & 0 & C_{44} & 0 & 0 \\ 0 & 0 & 0 & C_{55} & 0 \\ 0 & 0 & 0 & 0 & C_{66} \end{bmatrix}^{(k)} \tag{D3}$$

The explicit relations for C_{ij} in terms of engineering constants are given as

$$C_{11} = \frac{E_L}{(1 - \nu_{LT}\nu_{TL})}, \qquad C_{12} = \frac{\nu_{LT} E_T}{(1 - \nu_{LT}\nu_{TL})}$$

$$C_{22} = \frac{E_T}{(1 - \nu_{LT}\nu_{TL})}, \qquad C_{44} = G_{TT}$$

$$C_{55} = G_{LT}, \qquad C_{66} = G_{LT} \tag{D4}$$

The transformed material loss factors for the kth layer are defined as

$$[\bar{\eta}]^{(k)} = \begin{bmatrix} \bar{\eta}_{11} & \bar{\eta}_{12} & 0 & 0 & \bar{\eta}_{16} \\ \bar{\eta}_{21} & \bar{\eta}_{22} & 0 & 0 & \bar{C}_{26} \\ 0 & 0 & \bar{\eta}_{44} & \bar{\eta}_{45} & 0 \\ 0 & 0 & \bar{\eta}_{54} & \bar{\eta}_{55} & 0 \\ \bar{\eta}_{61} & \bar{\eta}_{62} & 0 & 0 & \bar{\eta}_{66} \end{bmatrix}^{(k)} \tag{D5}$$

where

$$[\bar{\eta}]^{(k)} = [R(-\theta_k)][\eta]^{(k)}[R(\theta_k)]^T \tag{D6}$$

and the material loss factors in principal axes are defined as

$$[\eta]^{(k)} = \begin{bmatrix} \eta_{11} & 0 & 0 & 0 & 0 \\ 0 & \eta_{22} & 0 & 0 & 0 \\ 0 & 0 & \eta_{44} & 0 & 0 \\ 0 & 0 & 0 & \eta_{55} & 0 \\ 0 & 0 & 0 & 0 & \eta_{66} \end{bmatrix}^{(k)} \tag{D7}$$

and explicit relations for η_i are

$$\eta_{11} = \eta_L, \qquad \eta_{22} = \eta_T, \qquad \eta_{44} = \eta_{TT}$$

$$\eta_{55} = \eta_{LT}, \qquad \eta_{66} = \eta_{LT} \tag{D8}$$

The transformation matrix $[R(\theta_k)]$ is defined as

$$[R(\theta_k)] = \begin{bmatrix} \cos^2\theta_k & \sin^2\theta_k & 0 & 0 & -\sin 2\theta_k \\ \sin^2\theta_k & \cos^2\theta_k & 0 & 0 & \sin 2\theta_k \\ 0 & 0 & \cos\theta_k & \sin\theta_k & 0 \\ 0 & 0 & -\sin\theta_k & \cos\theta_k & 0 \\ \sin\theta_k\cos\theta_k & -\sin\theta_k\cos\theta_k & 0 & 0 & \cos^2\theta_k - \sin^2\theta_k \end{bmatrix} \tag{D9}$$

Appendix E: Shape Functions

The shape functions are

$$\left[N_B^i\right] = \frac{1}{2A}\begin{bmatrix} b_i & 0 & 0 & 0 & 0 \\ 0 & b_i & 0 & 0 & 0 \\ c_i & 0 & 0 & 0 & 0 \\ 0 & c_i & 0 & 0 & 0 \\ 0 & 0 & (1/2A)b_jb_kq_{i,jk} & (1/2A)b_jb_kg_{i,jk} & (1/2A)b_jb_kh_{i,jk} \\ 0 & 0 & (1/2A)c_jc_kq_{i,jk} & (1/2A)c_jc_kg_{i,jk} & (1/2A)c_jc_kh_{i,jk} \\ 0 & 0 & (1/2A)b_jc_kq_{i,jk} & (1/2A)b_jc_kg_{i,jk} & (1/2A)b_jc_kh_{i,jk} \end{bmatrix} \tag{E1}$$

$$[N_B] = \left\lfloor N_B^1, N_B^2, N_B^3 \right\rfloor \tag{E2}$$

$$\left[N_S^i\right] = \begin{bmatrix} n_i & 0 & 0 & 0 & 0 \\ 0 & n_i & 0 & 0 & 0 \\ 0 & 0 & (1/2A)b_kq_{i,k} & (1/2A)b_kg_{i,k} & (1/2A)b_kh_{i,k} \\ 0 & 0 & (1/2A)c_kq_{i,k} & (1/2A)c_kg_{i,k} & (1/2Ac_kh_)i,k \end{bmatrix} \tag{E3}$$

$$[N_S] = \left[N_S^1, N_S^2, N_S^3\right] \tag{E4}$$

$$\left[N_\rho^i\right] = \begin{bmatrix} n_i & 0 & 0 & 0 & 0 \\ 0 & n_i & 0 & 0 & 0 \\ 0 & 0 & q_i & g_i & h_i \\ 0 & 0 & (1/2A)b_kq_{i,k} & (1/2A)b_kg_{i,k} & (1/2A)b_kh_{i,k} \\ 0 & 0 & (1/2A)c_kq_{i,k} & (1/2A)c_kg_{i,k} & (1/2A)c_kh_{i,k} \end{bmatrix} \tag{E5}$$

$$[N_\rho] = \left\lfloor N_\rho^1, N_\rho^2, N_\rho^3 \right\rfloor \tag{E6}$$

where i, j, and $k = 1, 2, 3$ and $(\,)_{,i} = \partial/\partial\zeta_i$, and $(\,)_{,ij} = \partial^2/\partial\zeta_i\partial\zeta_j$.

Acknowledgment

This work was supported by the Brain Korea 21 project.

References

[1]Yan, M. J., and Dowell, E. H., "Governing Equations for Vibrating Constrained-Layer Damping Sandwich Plates and Beams," *Journal of Applied Mechanics*, Vol. 39, Dec. 1972, pp. 1041–1047.

[2]Sadasiva Rao, Y. V. K., and Nakra, B. C., "Vibrations of Unsymmetrical Sandwich Beams and Plates with Viscoelastic Cores," *Journal of Sound and Vibration*, Vol. 34, No. 3, 1974, pp. 309–326.

[3]Douglas, B. E., and Yang, J. C. S., "Transverse Compressional Damping in the Vibratory Response of Elastic-Viscoelastic–Elastic Beams, *AIAA Journal*, Vol. 16, No. 9, 1978, pp. 925–930.

[4]Miles, R. N., and Reinhall, P. G., "An Analytical Model for the Vibration of Laminated Beams Including the Effects of Both Shear and Thickness Deformation in the Adhesive Layer," *Journal of Vibration, Acoustics, Stress, and Reliability in Design*, Vol. 108, Jan. 1986, pp. 56–64.

[5]Barrett, D. J., "An Anisotropic Laminated Damped Plate Theory," *Journal of Sound and Vibration*, Vol. 154, No. 3, 1992, pp. 453–465.

[6]Alam, N., and Asnani, N. T., "Vibration and Damping Analysis of Multilayered Rectangular Plates with Constrained Viscoelastic Layers," *Journal of Sound and Vibration*, Vol. 97, No. 4, 1984, pp. 597–614.

[7]Alam, N., and Asnani, N. T., "Refined Vibration and Damping Analysis of Multilayered Rectangular Plates," *Journal of Sound and Vibration*, Vol. 119, No. 2, 1987, pp. 347–362.

[8]Johnson, C. D., and Kienholz, D. A., "Finite Element Prediction of Damping in Structures with Constrained Viscoelastic Layers," *AIAA Journal*, Vol. 20, No. 9, 1982, pp. 1284–1290.

[9]Malhotra, S. K., Ganesan, N., and Veluswami, M. A., "Vibration and Damping Analysis of Orthotropic Triangular Plates," *Journal of Sound and Vibration*, Vol. 130, No. 3, 1989, pp. 379–386.

[10]Saravanos, D. A., and Pereira, J. M., "Effects of Interply Damping Layers on the Dynamic Characteristics of Composite Plates," *AIAA Journal*, Vol. 30, No. 12, 1992, pp. 2906–2913.

[11]Saravanos, D. A., "Analysis of Passive Damping in Thick Composite Structures," *AIAA Journal*, Vol. 31, No. 8, 1993, pp. 1503–1510.

[12]Di Sciuva, M., "Bending, Vibration and Buckling of Simply Supported Thick Multilayered Orthotropic Plates: An Evaluation of a New Displacement Model," *Journal of Sound and Vibration*, Vol. 105, No. 3, 1986, pp. 425–442.

[13]Di Sciuva, M., "An Improved Shear-Deformation Theory for Moderately Thick Multilayered Anisotropic Shells and Plates," *Journal of Applied Mechanics*, Vol. 54, Sept. 1987, pp. 589–596.

[14]Di Sciuva, M., "A General Quadrilateral Multilayered Plate Element with Continuous Interlaminar Stresses," *Computers and Structures*, Vol. 47, No. 1, 1993, pp. 91–105.

[15]Di Sciuva, M., "A Third-Order Triangular Multilayered Plate Finite Element with Continuous Interlaminar Stresses," *International Journal for Numerical Methods in Engineering*, Vol. 38, No. 1, 1995, pp. 1–26.

[16]Cho, M., and Parmerter, R. R., "Finite Element for Composite Plate Bending Based on Efficient Higher-Order Theory," *AIAA Journal*, Vol. 32, No. 11, 1994, pp. 2241–2248.

[17]Specht, B., "Modified Shape Functions for the Three-Node Plate Bending Element Passing the Patch Test," *International Journal for Numerical Methods in Engineering*, Vol. 26, No. 3, 1988, pp. 705–715.

[18]Lee, D. G., "Vibration and Stability Analysis of a Rotating Multi-Layer Annular Plate with a Stationary Load System," Ph.D. Dissertation, Dept. of Aerospace Engineering, Univ. of Michigan, Ann Arbor, MI, May 1996.

[19]Lee, D. G., and Waas, A. M., "Stress Analysis of Laminated Composite Annular Disks Subjected to a Concentrated Transverse Load Using Layer-Wise Zig-Zag Theory," *Advanced Composite Materials*, Vol. 6, No. 4, 1997, pp. 261–278.

[20]Lee, D. G., and Waas, A. M., "Stability Analysis of a Rotating Multi-Layer Annular Plate with a Stationary Frictional Follower Load," *International Journal of Mechanical Science*, Vol. 39, No. 10, 1997, pp. 1117–1138.

[21]Lee, D. G., Waas, A. M., and Karnopp, B. H., "Analysis of a Rotating Multi-Layer Annular Plate Modeled Via Layerwise Zig-Zag Theory: Free Vibration and Transient Analysis," *Computers and Structures*, Vol. 66, Nos. 2–3, 1998, pp. 313–335.

[22]Averill, R. C., "Static and Dynamic Response of Moderately Thick Laminated Beams with Damage," *Composites Engineering*, Vol. 4, No. 4, 1994, pp. 381–395.

[23]Averill, R. C., and Yip, Y. C., "Development of Simple, Robust Finite Elements Based on Refined Theories for Thick Laminated Beams," *Computers and Structures*, Vol. 59, No. 3, 1996, pp. 529–546.

[24]Lee, D. G., and Kosmatka, J. B., "Improved Layer-Wise Zig-Zag Theory and Finite Element for Composite Structures," *International Journal for Numerical Methods in Engineering* (to be published).

A. M. Waas
Associate Editor